ACS OMEGA

http://pubs.acs.org/journal/acsodf

Article

Unveiling Zwitterionization of Glycine in the Microhydration Limit

Ravi Tripathi,* Laura Durán Caballero, Ricardo Pérez de Tudela, Christoph Hölzl, and Dominik Marx

Cite This: *ACS Omega* 2021, 6, 12676−12683

Read Online

ACCESS | Metrics & More | Article Recommendations | Supporting Information

ABSTRACT: Charge separation under solvation stress conditions is a fundamental process that comes in many forms in doped water clusters. Yet, the mechanism of intramolecular charge separation, where constraints due to the molecular structure might be intricately tied to restricted solvation structures, remains largely unexplored. Microhydrated amino acids are such paradigmatic molecules. Ab initio simulations are carried out at 300 K in the frameworks of metadynamics sampling and thermodynamic integration to map the thermal mechanisms of zwitterionization using $Gly(H_2O)_n$ with n = 4 and 10. In both cases, a similar water-mediated proton transfer chain mechanism is observed; yet, detailed analyses of thermodynamics and kinetics demonstrate that the charge-separated zwitterion is the preferred species only for n = 10 mainly due to kinetic stabilization. Structural analyses disclose that bifurcated H-bonded water bridges, connecting the cationic and anionic sites in the fluctuating microhydration network at room temperature, are enhanced in the transition-state ensemble exclusively for n = 10 and become overwhelmingly abundant in the stable zwitterion. The findings offer potential insights into charge separation under solvation stress conditions beyond the present example.

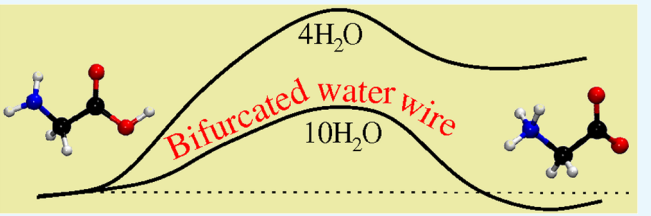

INTRODUCTION

Charge separation induced by water is among the fundamental processes in chemistry. A wealth of such processes is known, including but not limited to solvation of detached electrons and ion−electron pairs,[1−4] dissolution of salts,[5−7] self-ionization of water into the solvated proton and hydroxide,[8−12] or dissociation of acids,[13−15] which remain research topics of much current scientific interest. Common to all of them is the crucial role solvation plays foremost in the formation, but subsequently also in the stabilization of the charge-separated species by water. Both formation and stabilization of charges are advantageous if plenty of solvating water molecules are available, notably in bulk aqueous solution. The situation is radically different under the limit of having only a very few water molecules available: A piece of metallic sodium is known to most vigorously dissolve in a bucket of water by dissociating into $Na^+(aq)$ and $e^-(aq)$, while $Na(H_2O)_n$ are quite stable molecular complexes for sufficiently small cluster sizes n as shown by computation and experiment.[16−18] More recently, it has been shown that a minimum of four water molecules is required to dissociate a simple strong acid in the microhydration limit, $HCl(H_2O)_n$.[14,15,19−21]

While moving next to acids other than HCl is certainly appealing, a more complex situation is found in amino acids: They contain in one and the same molecule both the acidic proton-donating and the basic proton-receiving groups that are geometrically restrained by the molecular backbone. The well-known fact that amino acids exist in their neutral form in the gas phase, i.e., carrying charge-neutral −COOH and $-NH_2$ groups, but readily convert into their zwitterionic form in bulk water supports the key role of solvation water in the charge-separation process leading to zwitterionization and thus to charged $-COO^-$ and $-NH_3^+$ groups. So far, extensive efforts have been made to understand zwitterion formation of both microhydrated and bulk solvated glycine as the role model for amino acids.[22−43] Whereas zwitterionization of glycine is well studied in the bulk phase limit[29] including its hydration properties therein[34,43] (e.g., the first hydration shell of glycine in water is shown to be constituted by about 7−8 water molecules around its charged groups[34,43]), not much is known in the microhydration limit on how zwitterionization can occur in terms of the underlying proton transfers and, second, which factors are contributing to zwitterion stabilization. To answer these questions requires not only the full mechanistic understanding of zwitterion formation in the microhydrated environment as such but also knowledge of the thermodynamics and kinetics by contrasting the generic scenario when the zwitterion is only metastable compared to its global stability. Despite long-standing efforts and most valuable computational insights into the "static geometry optimization limit",[22,24−28,33,35−38,41,42] these important questions still remain open even for the simplest possible amino acid at finite temperatures.

Received: February 17, 2021
Accepted: March 24, 2021
Published: May 7, 2021

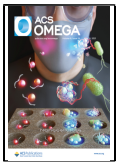

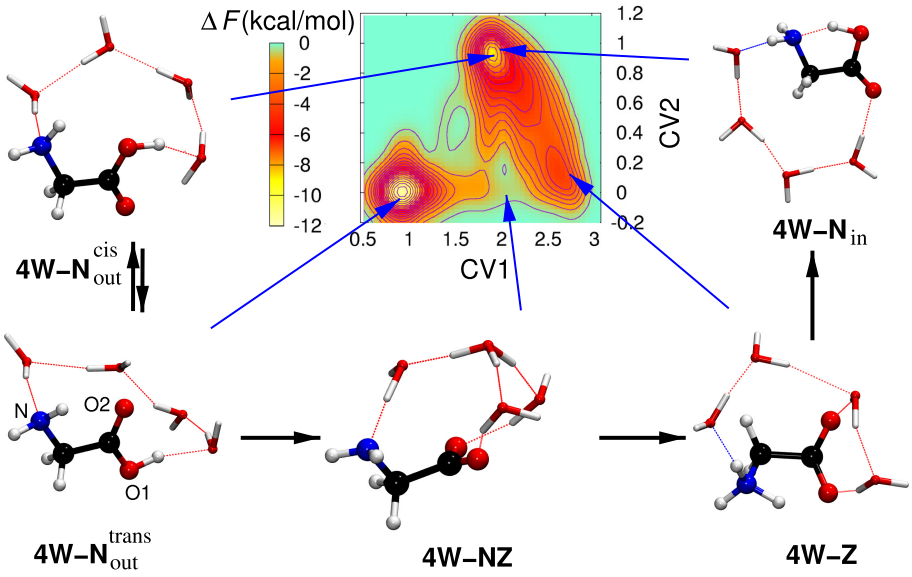

Figure 1. Free-energy surface at 300 K from ab initio metadynamics spanned by the generalized coordinates CV1 and CV2, see text, and representative configuration snapshots for neutral (N) ⇌ zwitterion (Z) interconversions for $Gly(H_2O)_4$; see text. The blue arrows mark the locations of the shown structures on the FES; note that the neutral 4W-N_{out}^{cis} and 4W-N_{in} conformers are indistinguishable in the (CV1, CV2) space, whereas the conformational difference between the 4W-N_{out}^{cis} and 4W-N_{out}^{trans} isomers is visualized in Figure S3.

In what follows, we are going to address these questions based on free-energy surfaces (FESs) computed at room temperature to reveal the thermal mechanism and free energy of charge separation in glycine in the restricted solvation environment that is provided if only a few water molecules are available. To this end, we considered two microsolvated structures, $Gly(H_2O)_4$ and $Gly(H_2O)_{10}$, since it has been shown[38] that the undissociated (neutral) and charge-separated (zwitterionic) forms of glycine are their respective globally stable states, whereas the situation is much less clear-cut[38] for intermediate sizes $4 < n < 10$ (as supported by new coupled cluster benchmark data; see SI Section 1 and Figure S1). Thus, contrasting these two limiting cases is expected to provide the most valuable insights into what finally favors zwitterionization in microhydrated $Gly(H_2O)_n$ clusters. To achieve this, we employed extensive ab initio molecular dynamics simulations[44] using the RPBE-D3 density functional (refer to SI Section 1 for validation of our methodology) together with metadynamics sampling and thermodynamic integration of the representative $n = 4$ and 10 clusters at 300 K (as detailed in the next section). We note at this early stage that the detailed picture of zwitterionization of microhydrated glycine thus obtained can be the basis for qualitatively rationalizing zwitterionization of other amino acids with neutral side chains, whereas such de/protonable functional groups will certainly add complexity. Moreover, our findings may not readily apply to biomacromolecules, such as polypeptides or proteins subject to solvation water restrictions, since the de/protonable terminal groups might be separated by large distances due to the presence of the backbone chain.

RESULTS AND DISCUSSION

We first investigated the thermal reaction pathways by which neutral structures of $Gly(H_2O)_4$ and $Gly(H_2O)_{10}$ could zwitterionize at 300 K, given only 4 or 10 solvating water molecules. This is done by computing the free-energy landscapes (see the Methods and Models section for details) using the following two very general (dimensionless) collective variables (CVs): CV1 is defined as the difference of the coordination number (refer to the Methods and Models section for its definition) of nitrogen to all hydrogen atoms in the cluster, $C[N-H_{all}]$, to the coordination number of O1, which lies in the trans position with respect to $-NH_2$ and carries the hydrogen in the initial neutral cluster (see Figure 1 for site labeling) again to all hydrogens present, $C[O1-H_{all}]$, while CV2 is the coordination number of the other oxygen (O2) to all hydrogen atoms, $C[O2-H_{all}]$. We emphasize that this CV space is very general since it allows for proton transfers from/to any water molecule present in the cluster, thus not biasing transfers by selecting only a subset of water molecules, and at the same time involves all de/protonable sites of glycine. Furthermore, we note that the metadynamics simulations were exclusively performed to qualitatively explore the topology of the free-energy landscape of zwitterionization, whereas all reported quantitative free-energy differences (see below) were obtained from converged ab initio thermodynamic integration calculations (see the Methods and Models section) along suitable one-dimensional pathways as determined from metadynamics. Therefore, no further attempts were made to assess the convergence of these qualitative metadynamics simulations as the converged free-energy profiles, and thus the reported free-energy differences were finally obtained from thermodynamic integration calculations.

On performing the FES mapping first with 4W-N_{out}, a proton shuttling between the two carboxyl oxygen atoms via a water molecule was observed resulting in cis and trans isomers, 4W-N_{out}^{cis} and 4W-N_{out}^{trans}, as indicated in Figure 1. These two isomers can be distinguished based on the location of protonated oxygen with respect to the $-NH_2$ group, which is located in the cis position in 4W-N_{out}^{cis} (corresponding to a dihedral torsional angle of $\theta(N-C-C-O_H) \approx 0°$) and the trans position in 4W-N_{out}^{trans} (where $\theta \approx 180°$) as visualized using Newman projections in Figure S3. It is reassuring to sample this transformation since the existence of these

https://doi.org/10.1021/acsomega.1c00869
ACS Omega 2021, 6, 12676−12683

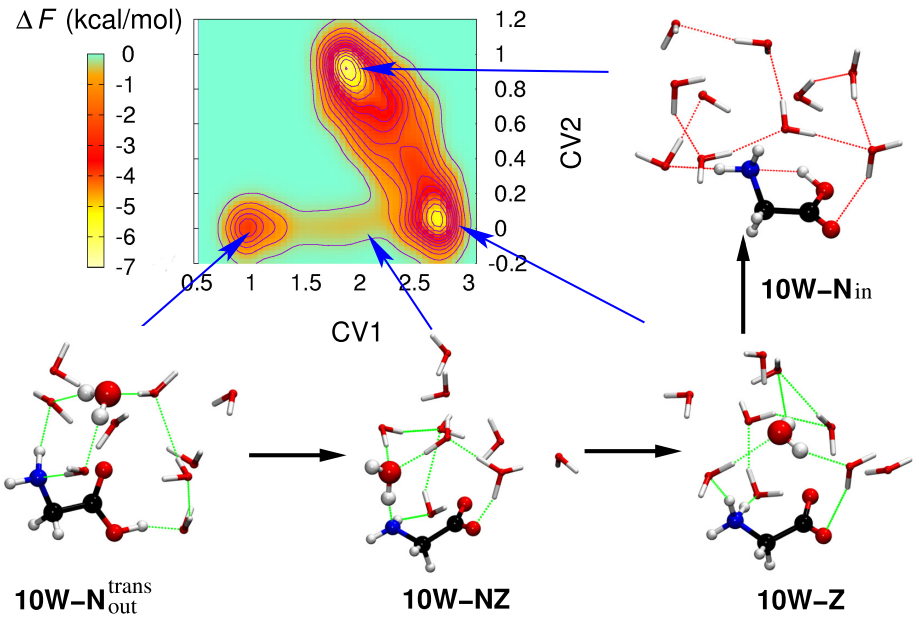

Figure 2. Free-energy surface at 300 K from ab initio metadynamics spanned by the generalized coordinates CV1 and CV2, see text, and representative configuration snapshots for neutral (N) ⇌ zwitterion (Z) interconversions for $Gly(H_2O)_{10}$; see text. The blue arrows mark the locations of the shown structures on the FES. The bifurcated H-bonded water bridge, see text, is depicted in 10W-N_{out}^{trans}, 10W-NZ, and 10W-Z by dashed green lines with the bifurcating H_2O molecule enhanced, whereas the other H-bonds present in these structures are not shown for clarity. The H-bonds in 10W-N_{in} are shown using dashed red lines instead.

particular cis and trans isomers of glycine has been found experimentally in the gas phase and also in the presence of one water molecule.[45−47] Our study, hence, shows that this isomerization can readily occur even in the presence of four microsolvating water molecules that clamp the carboxyl to the amino group. The neutral trans conformer, 4W-N_{out}^{trans}, is found to zwitterionize to yield 4W-Z via a water-mediated proton transfer from the carboxyl group to the amino group via three water molecules as depicted by the structure 4W-NZ. Interestingly, this metastable zwitterionic species 4W-Z can readily decay into another neutral species, 4W-N_{in}, via spontaneous direct proton transfer from its $-NH_3^+$ group to the neighboring oxygen of the carboxyl group, O2. This yields another conformer of neutral glycine in which the −COOH group points inward and donates an intramolecular H-bond to the amino group (see the 4W-N_{in} structure in Figure 1); note that our metadynamics simulation does not resolve the neutral 4W-N_{in} conformer from 4W-N_{out}^{cis}, which, however, does not impact on the free-energy profile of zwitterionization as reported below since that has been obtained using thermodynamic integration. The existence of this third neutral conformer was also experimentally observed[45,46,48] both for bare glycine in the gas phase as well as in Gly−water aggregates, which provides further confidence that our enhanced sampling approach faithfully maps the relevant conformational space.

In the case of 10W-N_{out} (see Figure 2), on the contrary, no proton exchange between the two oxygens of the carboxyl group was observed, indicating the existence of only the trans conformer in larger clusters. In retrospect, this is expected as the nonprotonated O2 oxygen in 10W-N_{out} is involved in H-bonding with surrounding water molecules and, therefore, it has a reduced tendency to attract the proton from the neighboring oxygen atom. This is in contrast to 4W-N_{out}, where fewer water molecules around glycine limit the formation of such charge-stabilizing H-bonding interactions. The zwitterion, 10W-Z in Figure 2, is generated from 10W-N_{out} by a proton transfer cascade from the carboxyl oxygen to the amine nitrogen again via a chain of three water molecules as caught by the representative configuration 10W-NZ. Similar to what is observed in $Gly(H_2O)_4$, a proton transfer from $-NH_3^+$ to the carboxyl oxygen O2 interconverting 10W-Z into the neutral 10W-N_{in} species (see Figure 2) is possible, yet only after surmounting a free-energy barrier.

Given the similarities observed in the thermal reaction pathways for charge separation (i.e., $N_{out} \rightarrow Z$) in $Gly(H_2O)_4$ and $Gly(H_2O)_{10}$ at 300 K, which are disclosed here for the first time, it is interesting to ask if the corresponding relative stabilities (i.e., thermodynamics) and energy barriers (i.e., kinetics) are also comparable. For this purpose, well-converged free-energy profiles have been computed for the $N_{out} \rightarrow Z$ zwitterionization of glycine using $n = 4$ and 10 water molecules by employing ab initio thermodynamic integration, the details of which can be found in SI Section 2. For $n = 4$, the thermal activation free energy for 4W-$N_{out} \rightarrow$ 4W-Z zwitterionization is about 12 kcal/mol, whereas the reverse barrier is only ≈4 kcal/mol (see Figure 3). Thus, the neutral $Gly(H_2O)_4$ cluster is thermodynamically substantially more stable compared to its zwitterionic state. For $n = 10$, on the other hand, the forward and reverse barriers for the 10W-$N_{out} \rightarrow$ 10W-Z process are around 6 and 7 kcal/mol, respectively, implying that the zwitterionic state is thermodynamically stabilized by ≈1 kcal/mol (see Figure 3); note that these thermal free-energy differences between neutral and zwitterionic species at 300 K are in qualitative agreement for both cluster sizes, $n = 4$ and 10, with the previously reported SCS-MP2 potential energy differences including zero-point vibrational corrections.[38] In conclusion, the charge-separated zwitterionic state is (marginally) stabilized for the larger microsolvated cluster, $Gly(H_2O)_{10}$, whereas the smaller cluster, $Gly(H_2O)_4$, prefers the neutral state at the level of thermodynamic stabilities at 300 K.

https://doi.org/10.1021/acsomega.1c00869
ACS Omega 2021, 6, 12676−12683

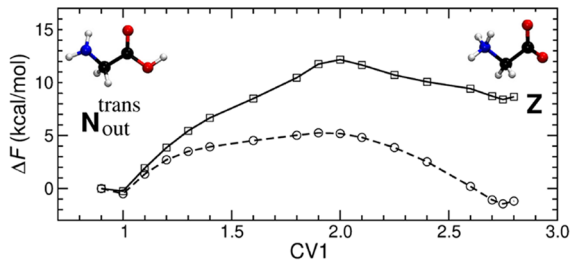

Figure 3. Free-energy profiles at 300 K from ab initio thermodynamic integration along the generalized coordinate CV1, see text and SI, for the 4W-N_{out} ⇌ 4W-Z (solid line with squares) and 10W-N_{out} ⇌ 10W-Z (dashed line with circles) neutral (N) ⇌ zwitterion (Z) interconversion processes. The left and right insets depict glycine itself in the corresponding neutral and zwitterionic states, respectively.

It now appears puzzling that the relative overall stabilities of the neutral and charge-separated states are different for $Gly(H_2O)_n$, given that the interconversion mechanisms are so similar for n = 4 and 10. Based on static optimizations of a vast ensemble of $Gly(H_2O)_n$ ground-state structures, it has been found[38] that a specific topological feature—namely, a bifurcated H-bonded water bridge, which, in addition to directly connecting the two functional groups, also connects the amino group to itself via a bifurcating water molecule—is required to render the zwitterion the global potential energy minimum (i.e., in the static 0 K limit and without providing any insights whatsoever into the charge-separation mechanism itself). At room temperature, however, H-bonded water networks are known to significantly fluctuate due to thermally driven H-bond breaking and making processes.[49] Thus, is there any hope that such bifurcated H-bonded water wires, being fragile features of H-bond networks, can be the answer? First of all, analyses of configurations underlying the free-energy surfaces show that the water molecules form an extended H-bond network that connects the two terminal groups in all cases (as visualized by the representative configurations in Figures 1 and 2 and statistically analyzed in Figure S12). Second, however, only in the 10W-N_{out} to 10W-Z transformation process favoring the zwitterion is the presence of bifurcated H-bonded water bridges observed as shown in the snapshots in Figure 2. These bifurcated water wires are present in the n = 10 reactant state ensemble, slightly increase in number in the transition-state ensemble, and finally clearly dominate the H-bonding topology in the product state ensemble (see Figure S12 for quantitative analysis). The nontrivial finding is that this very topological feature of the microhydrating H-bond network is decisive for successful zwitterionization not only in the computational static zero Kelvin limit but also under realistic finite-temperature conditions where pronounced thermal fluctuations at 300 K induce enhanced H-bond dynamics.

For both cluster sizes, n = 4 and 10, the generation of nW-N_{in} from nW-Z opens up a new pathway for zwitterion to neutral transformation: Instead of nW-Z transforming into nW-N_{out} via the aforementioned water-mediated proton transfer chain, a direct proton transfer from $-NH_3^+$ to the O2 site of $-COO^-$ in nW-Z leads to another neutral conformation, nW-N_{in}. To determine the kinetic feasibility of this proton transfer pathway as well as the thermodynamic stability of nW-N_{in} with respect to nW-Z, we calculated the associated free-energy barriers for n = 4 and 10 as detailed in SI Section 3. The free-energy barrier for 4W-Z → 4W-N_{in} was obtained to be only ≈1 kcal/mol, while the reverse activation free energy is around 4 kcal/mol (see Figures 4 and S7). Similarly, the forward and

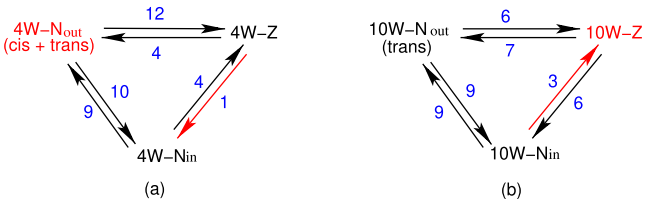

Figure 4. Free-energy barriers at 300 K from ab initio thermodynamic integration for conformational interconversions in (a) $Gly(H_2O)_4$ and (b) in $Gly(H_2O)_{10}$ in kcal/mol; note that k_BT at 300 K corresponds to 0.6 kcal/mol. The thermodynamically stable states as well as the kinetically preferred pathways for charge recombination Z → N in (a) and for zwitterionization N → Z in (b) are highlighted in red.

reverse barriers for 10W-Z ⇌ 10W-N_{in} interconversion are roughly 6 and 3 kcal/mol, respectively (see Figures 4 and S7). However, 10W-Z is thermodynamically only marginally stabilized by ≈1 kcal/mol with reference to the neutral 10W-N_{out} species. Together, these results show that the zwitterionic state of $Gly(H_2O)_{10}$ is essentially only kinetically stabilized with respect to its neutral form. In contrast, the charge-separated 4W-Z state cannot be trapped at all since it is both thermodynamically and kinetically disfavored. These findings based on free-energy analyses were furthermore confirmed by running unbiased ab initio trajectory calculations of the 4W-Z and 10W-Z structures (refer to SI Section 3 for supporting data). Besides, we also scrutinized whether another interconversion channel is possible, involving the neutral N_{in} isomers instead (see SI Section 4). The computed free energetics, however, rule out kinetically favorable detour pathways for Z to N_{out} transformation via the N_{in} intermediate for both microhydration numbers (see Figures 4 and S11). Overall, all of these analyses provide substantial evidence that the charge-separated zwitterionic form of $Gly(H_2O)_{10}$ is preferred under ambient gas-phase conditions mainly as a result of kinetic stabilization (since the lowest free-energy barrier for the neutral to zwitterion transformation is only 3 kcal/mol but twice as high for the lowest-energy reverse process), whereas the neutral form of $Gly(H_2O)_4$ is overwhelmingly populated at equilibrium since it is both thermodynamically and kinetically favored.

Let us finally connect our findings on glycine microsolvation under ambient conditions to bulk solvation.[29] Unsurprisingly, water-mediated zwitterionization is also found in bulk solution, but now the charge-separated state is also thermodynamically stabilized by as much as about 10 kcal/mol (instead of being marginally stabilized by only ≈1 kcal/mol with n = 10 water molecules) together with an even slightly lower kinetic barrier of roughly 2 kcal/mol (versus ≈3 kcal/mol) to generate the zwitterion; recall that the thermal energy, k_BT, is 0.6 kcal/mol at 300 K. This allows us to disclose the full sequence at room temperature from a situation where (i) zwitterionic glycine is both thermodynamically and kinetically unstable if too few water molecules are available (n = 4), to a scenario where (ii) the charge-separated state is mainly kinetically stabilized with more water molecules (n = 10), to the limit where (iii) the zwitterion is both thermodynamically and kinetically stabilized (n → ∞).

https://doi.org/10.1021/acsomega.1c00869
ACS Omega 2021, 6, 12676−12683

CONCLUSIONS AND OUTLOOK

In this work, we have determined the reaction pathways for intramolecular charge separation at finite temperature in two microsolvated amino acid clusters, namely, $Gly(H_2O)_4$ and $Gly(H_2O)_{10}$, through extensive ab initio simulations under ambient conditions. For both microhydration scenarios, the conversion of neutral into zwitterionic glycine takes place via a proton transfer cascade from the carboxyl to the amino group employing a short water wire. On comparing the free-energy barriers for all involved reactions as well as the relative free energies of the zwitterion with respect to neutral species, we demonstrate that the zwitterionic form of $Gly(H_2O)_{10}$ is thermodynamically only marginally stable at room temperature but kinetically stabilized, whereas it is the neutral form of the smaller cluster that is both thermodynamically and kinetically favored. The key feature allowing for sustained charge separation in the microhydration limit is revealed to be the formation of a specific topological feature of the H-bonding network. This is the establishment of bifurcated water bridges between the positively and negatively charged functional groups that are enhanced even at room temperature in the transition-state ensemble only for $n = 10$, and finally dominate over linear water wires in the fully charge-separated state. Bifurcated water bridges can only be built if a sufficient number of H-bonding water molecules is available beyond merely solvating the two charged groups by themselves. Overall, our study provides possible generic insights into zwitterionization of glycine and, as such, can be applied toward understanding charge-separation processes in other cases where both steric constraints and solvation stress are operational. Finally, it would be interesting to see in future studies how the presence of additional de/protonable groups in amino acids might impact the overall charge-separation mechanisms.

METHODS AND MODELS

System Setup and Computational Details. The minimum energy structures that correspond to the neutral and zwitterionic forms of $Gly(H_2O)_4$ and $Gly(H_2O)_{10}$, respectively, as reported in our previous work[38] were considered as the initial structures to launch the present ab initio molecular dynamics (AIMD) simulations.[44] The neutral and zwitterionic structures of $Gly(H_2O)_4$/$Gly(H_2O)_{10}$ will be denoted 4W-N_{out}/10W-N_{out} and 4W-Z/10W-Z, respectively. In addition, a minimum energy structure of one other conformer of the neutral form, where the −COOH group is rotated inward and forms a H-bond interaction with $-NH_2$, was equilibrated and is denoted 4W-N_{in}/10W-N_{in} for $Gly(H_2O)_4$/$Gly(H_2O)_{10}$.

All simulations were performed using the CP2k suite of programs[50,51] that implements iterative Born−Oppenheimer propagation[44] to solve the electronic structure on the fly. The system was treated by density functional theory using the RPBE functional[52] supplemented by the D3 dispersion correction[53] (where the two-body terms together with zero damping are used) to account for the London (a.k.a. van der Waals) interactions. We chose the TZV2P triple-ζ Gaussian basis set with polarization functions[54] together with a plane wave cutoff of 500 Ry to represent the electron density, and the core electrons were described using norm-conserving separable dual-space Gaussian pseudopotentials.[55,56] A rather large simulation box of size $(21 \times 21 \times 21)$ Å^3 was considered in this study for all reported simulations, and the Martyna−Tuckerman Poisson solver[57] was used to apply finite-size rather than periodic boundary conditions. This is mandatory to fully suppress the long-range electrostatic interactions as required to properly compare free energies of zwitterionic versus the neutral $Gly(H_2O)_n$ clusters on equal footing. The temperature corresponding to 300 K was maintained using Nosé−Hoover chain thermostats.[58] A time step of 0.5 fs was chosen to integrate the equations of motion.

Free-Energy Sampling. The reaction pathways for the interconversion between different isomers were obtained by performing extended Lagrangian ab initio metadynamics simulations[59,60] using the same RPBE-D3 electronic structure method as that introduced in the previous subsection. Metadynamics is a powerful technique where sampling is enhanced in a space spanned by a set of predefined generalized coordinates, called the collective variables or CVs, which are assumed to provide a suitable coarse-grained description of the relevant free-energy subspace that describes all relevant rare events at the selected simulation temperature. To this end, a bias potential in terms of Gaussian hills is added to these CVs, which prevent the system from revisiting the already sampled points in the configurational space and by doing so allowing the system to visit unexplored regions including high (free)-energy regions corresponding to rare events. This eventually drives the system to escape the reactant minima via the lowest saddle point, enabling the reaction pathway to be determined. Additionally, an estimate of the underlying free-energy surface within the respective multidimensional CV subspace can be mapped out using the negative sum of the added biasing potentials. The interested reader can find more background and information on metadynamics sampling, for instance, in refs 44, 61−63.

We mainly used dimensionless CVs defined in terms of coordination numbers C

$$C[\mathrm{A}-\mathrm{B}] = \sum_{J\in \mathrm{B}} \frac{1-\left(\frac{d[\mathrm{A}-J]}{d^0_{\mathrm{AB}}}\right)^p}{1-\left(\frac{d[\mathrm{A}-J]}{d^0_{\mathrm{AB}}}\right)^{p+q}} \quad (1)$$

between a specific atom of species A and a set of other atoms J that belong to species B depending on their internuclear distance $d[\mathrm{A}-J]$. Here, d^0_{AB} is a fixed parameter that is defined based on the nature of interactions of the involved atoms, whereas p and q are integers that determine the steepness of the coordination number function. The value of d^0_{AB} was chosen to be 1.3 Å in all simulations, whereas the values of both p and q were set to 12.

A Gaussian potential of height $\approx$1.0 k_BT and width $\delta = 0.03$ was used to fill the minima. To avoid the well-known "hill-surfing" problem in metadynamics,[64] we employed the adaptive time step approach, where a new Gaussian is added only after a displacement in CV space that exceeds $1.5 \times \delta$ with respect to the center of previously added Gaussian.[64] A mass of 50 amu was assigned to the CV, and a coupling parameter of 2.0 au was selected in the extended Lagrangian.[60] The CV temperature is maintained at 300 K via scaling with the accepted tolerance of ±200 K. These parameters have been validated in a set of previous studies where similar Grotthuss-like proton transfer reactions involving water molecules were scrutinized.[29,65−68]

Although metadynamics can be efficiently used for both accelerating rare events and reconstructing high-dimensional

https://doi.org/10.1021/acsomega.1c00869
ACS Omega 2021, 6, 12676−12683

free-energy landscapes, the accuracy of the obtained free-energy difference and barrier estimates versus the underlying computational effort is a matter of concern.[61,62] An accurate description of barriers can only be achieved either by sampling many recrossing events involving all free-energy minima within the reaction subspace spanned by the respective CVs,[61,62] which is difficult or impossible to achieve on complex landscapes, or by performing well-tempered metadynamics where the growth rate of the bias potential is systematically decreased with simulation time,[69] where sampling becomes increasingly less efficient. In practice, both procedures are computationally demanding if the aim is to faithfully determine free-energy differences.

An alternative way to more easily obtain accurate estimates of free-energy differences along a one-dimensional transformation pathway only is to employ the traditional umbrella sampling[70] or thermodynamic integration (or potential of mean force)[71] methods along a predefined order parameter, which can be a typical CV, that connects the initial to the final state via a transition state. Therefore, in this work, instead of trying to quantitatively compute free-energy differences using metadynamics techniques, we employed ab initio thermodynamic integration[44] along a single CV. This was possible since analysis of the free-energy surfaces as obtained from ab initio metadynamics for both $Gly(H_2O)_4$ and $Gly(H_2O)_{10}$ revealed that orthogonal contributions to the interconversion of neutral and zwitterionic states as described by CV1 alone are very small according to Figures 1 and 2 in the main text. For this purpose, multiple initial configurations along CV1 as given by the respective free-energy surfaces obtained from metadynamics were sampled; see SI Section 2 for definitions of CV1 and CV2. For each such configuration, a usual constrained ab initio simulation[44] at a fixed λ = CV1 value (of at least 50 ps length) was performed to provide a converged average $\langle f \rangle_\lambda$ of the force acting on the constraint for that particular constraint (after excluding the first 5 ps). The resulting one-dimensional free-energy profiles are calculated from

$$\Delta F = -\int_a^b \langle f \rangle_\lambda \mathrm{d}\lambda \tag{2}$$

after integrating the average constraint force from the respective initial to the final state.

■ ASSOCIATED CONTENT

Supporting Information

The Supporting Information is available free of charge at https://pubs.acs.org/doi/10.1021/acsomega.1c00869.

Validation of the electronic structure method; details of calculations of free-energy barriers for the *n*W-Z ⇌ *n*W-N_{out} interconversions; details of mechanism and free-energy barriers for *n*W-Z ⇌ *n*W-N_{in} and *n*W-N_{in} ⇌ *n*W-N_{out} interconversions; and analyses of bifurcated H-bonded water bridges (PDF)

■ AUTHOR INFORMATION

Corresponding Author

Ravi Tripathi − *Lehrstuhl für Theoretische Chemie, Ruhr-Universität Bochum, 44780 Bochum, Germany;* orcid.org/0000-0002-8134-9954; Email: ravi.tripathi@theochem.rub.de

Authors

Laura Durán Caballero − *Lehrstuhl für Theoretische Chemie, Ruhr-Universität Bochum, 44780 Bochum, Germany*

Ricardo Pérez de Tudela − *Lehrstuhl für Theoretische Chemie, Ruhr-Universität Bochum, 44780 Bochum, Germany;* orcid.org/0000-0002-0314-6983

Christoph Hölzl − *Lehrstuhl für Theoretische Chemie, Ruhr-Universität Bochum, 44780 Bochum, Germany*

Dominik Marx − *Lehrstuhl für Theoretische Chemie, Ruhr-Universität Bochum, 44780 Bochum, Germany*

Complete contact information is available at: https://pubs.acs.org/10.1021/acsomega.1c00869

Notes

The authors declare no competing financial interest.

■ ACKNOWLEDGMENTS

This work was funded by the Deutsche Forschungsgemeinschaft (DFG, German Research Foundation) under Germany's Excellence Strategy—EXC 2033—390677874—RESOLV, as well as by the individual DFG grants MA 1547/11-2 and MA 1547/15 to D.M. Computational resources have been provided by HPC−RESOLV, HPC@ZEMOS, and BOVILAB@RUB.

■ REFERENCES

(1) Donald, W. A.; Demireva, M.; Leib, R. D.; Aiken, M. J.; Williams, E. R. Electron Hydration and Ion-Electron Pairs in Water Clusters Containing Trivalent Metal Ions. *J. Am. Chem. Soc.* **2010**, *132*, 4633−4640.

(2) Young, R. M.; Neumark, D. M. Dynamics of Solvated Electrons in Clusters. *Chem. Rev.* **2012**, *112*, 5553−5577.

(3) Herbert, J. M.; Coons, M. P. The hydrated electron. *Annu. Rev. Phys. Chem.* **2017**, *68*, 447−472.

(4) Yamamoto, Y.-i.; Suzuki, T. Ultrafast Dynamics of Water Radiolysis: Hydrated Electron Formation, Solvation, Recombination, and Scavenging. *J. Phys. Chem. Lett.* **2020**, *11*, 5510−5516.

(5) Dedonder-Lardeux, C.; Grégoire, G.; Jouvet, C.; Martrenchard, S.; Solgadi, D. Charge Separation in Molecular Clusters: Dissolution of a Salt in a Salt-$(Solvent)_n$ Cluster. *Chem. Rev.* **2000**, *100*, 4023−4038.

(6) Hou, G.-L.; Liu, C.-W.; Li, R.-Z.; Xu, H.-G.; Gao, Y. Q.; Zheng, W.-J. Emergence of Solvent-Separated Na^+−Cl^- Ion Pair in Salt Water: Photoelectron Spectroscopy and Theoretical Calculations. *J. Phys. Chem. Lett.* **2017**, *8*, 13−20.

(7) Zhang, C.; Giberti, F.; Sevgen, E.; de Pablo, J. J.; Gygi, F.; Galli, G. Dissociation of salts in water under pressure. *Nat. Commun.* **2020**, *11*, No. 3037.

(8) Marx, D. Proton Transfer 200 Years after von Grotthuss: Insights from Ab Initio Simulations. *ChemPhysChem* **2006**, *7*, 1848−1870.

(9) Marx, D.; Chandra, A.; Tuckerman, M. E. Aqueous Basic Solutions: Hydroxide Solvation, Structural Diffusion, and Comparison to the Hydrated Proton. *Chem. Rev.* **2010**, *110*, 2174−2216.

(10) Agmon, N.; Bakker, H. J.; Campen, R. K.; Henchman, R. H.; Pohl, P.; Roke, S.; Thämer, M.; Hassanali, A. Protons and Hydroxide Ions in Aqueous Systems. *Chem. Rev.* **2016**, *116*, 7642−7672.

(11) Moqadam, M.; Lervik, A.; Riccardi, E.; Venkatraman, V.; Alsberg, B. K.; van Erp, T. S. Local initiation conditions for water autoionization. *Proc. Natl. Acad. Sci. U.S.A.* **2018**, *115*, E4569−E4576.

(12) Rozsa, V.; Pan, D.; Giberti, F.; Galli, G. Ab initio spectroscopy and ionic conductivity of water under Earth mantle conditions. *Proc. Natl. Acad. Sci. U.S.A.* **2018**, *115*, 6952−6957.

(13) Rini, M.; Magnes, B.-Z.; Pines, E.; Nibbering, E. T. J. Real-Time Observation of Bimodal Proton Transfer in Acid-Base Pairs in Water. *Science* **2003**, *301*, 349−352.

(14) Gutberlet, A.; Schwaab, G.; Birer, Ö.; Masia, M.; Kaczmarek, A.; Forbert, H.; Havenith, M.; Marx, D. Aggregation-Induced

Dissociation of $HCl(H_2O)_4$ Below 1 K: The Smallest Droplet of Acid. *Science* **2009**, *324*, 1545−1548.
(15) Mani, D.; Pérez de Tudela, R.; Schwan, R.; Pal, N.; Körning, S.; Forbert, H.; Redlich, B.; van der Meer, A. F. G.; Schwaab, G.; Marx, D.; Havenith, M. Acid solvation versus dissociation at "stardust conditions": Reaction sequence matters. *Sci. Adv.* **2019**, *5* (6), No. eaav8179.
(16) Trenary, M.; Schaefer, H. F., III; Kollman, P. A novel class of molecular complexes: lithium-ammonia, lithium-water, lithium-hydrofluoric acid, lithium-hydrogen sulfide, sodium-water, and sodium-hydrofluoric acid. *J. Am. Chem. Soc.* **1977**, *99*, 3885−3886.
(17) Schulz, C. P.; Haugstätter, R.; Tittes, H. U.; Hertel, I. V. Free Sodium-Water Clusters. *Phys. Rev. Lett.* **1986**, *57*, 1703.
(18) Barnett, R. N.; Landman, U. Hydration of Sodium in Water Clusters. *Phys. Rev. Lett.* **1993**, *70*, 1775.
(19) Letzner, M.; Gruen, S.; Habig, D.; Hanke, K.; Endres, T.; Nieto, P.; Schwaab, G.; Walewski, Ł.; Wollenhaupt, M.; Forbert, H.; Marx, D.; Havenith, M. High resolution spectroscopy of HCl-water clusters: IR bands of undissociated and dissociated clusters revisited. *J. Chem. Phys.* **2013**, *139*, No. 154304.
(20) Pérez de Tudela, R.; Marx, D. Acid Dissociation in HCl-Water Clusters is Temperature Dependent and Cannot be Detected Based on Dipole Moments. *Phys. Rev. Lett.* **2017**, *119*, No. 223001.
(21) Pérez de Tudela, R.; Marx, D. Generating Excess Protons in Microsolvated Acid Clusters under Ambient Conditions: An Issue of Configurational Entropy versus Internal Energy. *Chem. - Eur. J.* **2020**, *26*, 11955−11959.
(22) Jensen, J. H.; Gordon, M. S. On the Number of Water Molecules Necessary To Stabilize the Glycine Zwitterion. *J. Am. Chem. Soc.* **1995**, *117*, 8159−8170.
(23) Xu, S.; Nilles, J. M.; Bowen, K. H., Jr. Zwitterion formation in hydrated amino acid, dipole bound anions: How many water molecules are required? *J. Chem. Phys.* **2003**, *119*, 10696−10701.
(24) Ramaekers, R.; Pajak, J.; Lambie, B.; Maes, G. Neutral and zwitterionic glycine.H_2O complexes: A theoretical and matrix-isolation Fourier transform infrared study. *J. Chem. Phys.* **2004**, *120*, 4182−4193.
(25) Aikens, C. M.; Gordon, M. S. Incremental Solvation of Nonionized and Zwitterionic Glycine. *J. Am. Chem. Soc.* **2006**, *128*, 12835−12850.
(26) Park, S.-W.; Im, S.; Lee, S.; Desfrançois, C. Structure and Stability of Glycine-$(H_2O)_3$ Cluster and Anion: Zwitterion vs. Canonical Glycine. *Int. J. Quantum Chem.* **2007**, *107*, 1316−1327.
(27) Bachrach, S. M. Microsolvation of Glycine: A DFT Study. *J. Phys. Chem. A* **2008**, *112*, 3722−3730.
(28) Kim, J.-Y.; Im, S.; Kim, B.; Desfrançois, C.; Lee, S. Structures and energetics of Gly-$(H_2O)_5$: Thermodynamic and kinetic stabilities. *Chem. Phys. Lett.* **2008**, *451*, 198−203.
(29) Nair, N. N.; Schreiner, E.; Marx, D. Peptide Synthesis in Aqueous Environments: The Role of Extreme Conditions on Amino Acid Activation. *J. Am. Chem. Soc.* **2008**, *130*, 14148−14160.
(30) Takayanagi, T.; Yoshikawa, T.; Kakizaki, A.; Shiga, M.; Tachikawa, M. Molecular dynamics simulations of small glycine−$(H_2O)_n$ (n= 2−7) clusters on semiempirical PM6 potential energy surfaces. *J. Mol. Struct.: THEOCHEM* **2008**, *869*, 29−36.
(31) Yoshikawa, T.; Motegi, H.; Kakizaki, A.; Takayanagi, T.; Shiga, M.; Tachikawa, M. Path-integral molecular dynamics simulations of glycine·$(H_2O)_n$ (n= 1−7) clusters on semi-empirical PM6 potential energy surfaces. *Chem. Phys.* **2009**, *365*, 60−68.
(32) Tian, S. X.; Sun, X.; Cao, R.; Yang, J. Thermal Stabilities of the Microhydrated Zwitterionic Glycine: A Kinetics and Dynamics Study. *J. Phys. Chem. A* **2009**, *113*, 480−483.
(33) Lee, K. T.; Han, K. Y.; Oh, I.; Kim, S. K. Barrierless pathways in the neutral-zwitterion transition of amino acid: Glycine-$(H_2O)_9$. *Chem. Phys. Lett.* **2010**, *495*, 14−16.
(34) Sun, J.; Bousquet, D.; Forbert, H.; Marx, D. Glycine in aqueous solution: solvation shells, interfacial water, and vibrational spectroscopy from ab initio molecular dynamics. *J. Chem. Phys.* **2010**, *133*, No. 114508.
(35) Kayi, H.; Kaiser, R. I.; Head, J. D. A theoretical investigation of the relative stability of hydrated glycine and methylcarbamic acid-from water clusters to interstellar ices. *Phys. Chem. Chem. Phys.* **2012**, *14*, 4942−4958.
(36) Meng, X.-J.; Zhao, H.-L.; Ju, X.-S. Influences of n (2−5) water molecules on the proton transfer in hydrated glycine complexes. *Comput. Theor. Chem.* **2012**, *1001*, 26−32.
(37) Kim, J.-Y.; Ahn, D.-S.; Park, S.-W.; Lee, S. Gas phase hydration of amino acids and dipeptides: effects on the relative stability of zwitterion vs. canonical conformers. *RSC Adv.* **2014**, *4*, 16352−16361.
(38) Pérez de Tudela, R.; Marx, D. Water-Induced Zwitterionization of Glycine: Stabilization Mechanism and Spectral Signatures. *J. Phys. Chem. Lett.* **2016**, *7*, 5137−5142.
(39) Xu, W.; Zhu, Q.; Hu, C. The Structure of Glycine Dihydrate: Implications for the Crystallization of Glycine from Solution and Its Structure in Outer Space. *Angew. Chem., Int. Ed.* **2017**, *129*, 2062−2066.
(40) Kim, Y.; Kim, J.; Baek, K. Y.; Kim, W. Y. Efficient structural elucidation of microhydrated biomolecules through the interrogation of hydrogen bond networks. *Phys. Chem. Chem. Phys.* **2018**, *20*, 8185−8191.
(41) Gochhayat, J. K.; Dey, A.; Pathak, A. K. An ab iniio study on the micro-solvation of amino acids: On the number of water molecules necessary to stabilize the zwitter ion. *Chem. Phys. Lett.* **2019**, *716*, 93−101.
(42) Sun, J.; Xu, Z.; Liu, X. Structures and stabilities of glycine and water complexes. *Chem. Phys.* **2020**, *528*, No. 110528.
(43) Di Gioacchino, M.; Ricci, M. A.; Imberti, S.; Holzmann, N.; Bruni, F. Hydration and aggregation of a simple amino acid: The case of glycine. *J. Mol. Liq.* **2020**, *301*, No. 112407.
(44) Marx, D.; Hutter, J. *International Series of Monographs on Chemistry*; Cambridge University Press, 2009.
(45) Reva, I. D.; Plokhotnichenko, A. M.; Stepanian, S. G.; Ivanov, A. Y.; Radchenko, E. D.; Sheina, G. G.; Blagoi, Y. P. The rotamerization of conformers of glycine isolated in inert gas matrices. An infrared spectroscopic study. *Chem. Phys. Lett.* **1995**, *232*, 141−148.
(46) Stepanian, S. G.; Reva, I. D.; Radchenko, E. D.; Rosado, M. T. S.; Duarte, M. L. T. S.; Fausto, R.; Adamowicz, L. Matrix-Isolation Infrared and Theoretical Studies of the Glycine Conformers. *J. Phys. Chem. A* **1998**, *102*, 1041−1054.
(47) Balabin, R. M. The First Step in Glycine Solvation: The Glycine-Water Complex. *J. Phys. Chem. B* **2010**, *114*, 15075−15078.
(48) Kaufmann, M.; Leicht, D.; Schwan, R.; Mani, D.; Schwaab, G.; Havenith, M. Helium droplet infrared spectroscopy of glycine and glycine-water aggregates. *Phys. Chem. Chem. Phys.* **2016**, *18*, 28082−28090.
(49) Ohmine, I.; Tanaka, H. Fluctuation, Relaxations, and Hydration in Liquid Water. Hydrogen-Bond Rearrangement Dynamics. *Chem. Rev.* **1993**, *93*, 2545−2566.
(50) Hutter, J.; Iannuzzi, M.; Schiffmann, F.; VandeVondele, J. CP2K: atomistic simulations of condensed matter systems. *Wiley Interdiscip. Rev.: Comput. Mol. Sci.* **2014**, *4*, 15−25.
(51) CP2k Developers Group. www.cp2k.org.
(52) Hammer, B.; Hansen, L. B.; Nørskov, J. K. Improved adsorption energetics within density-functional theory using revised Perdew-Burke-Ernzerhof functionals. *Phys. Rev. B* **1999**, *59*, 7413.
(53) Grimme, S.; Antony, J.; Ehrlich, S.; Krieg, H. A consistent and accurate ab initio parametrization of density functional dispersion correction (DFT-D) for the 94 elements H-Pu. *J. Chem. Phys.* **2010**, *132*, No. 154104.
(54) VandeVondele, J.; Hutter, J. Gaussian basis sets for accurate calculations on molecular systems in gas and condensed phases. *J. Chem. Phys.* **2007**, *127*, No. 114105.
(55) Goedecker, S.; Teter, M.; Hutter, J. Separable dual-space Gaussian pseudopotentials. *Phys. Rev. B* **1996**, *54*, 1703.
(56) Hartwigsen, C.; Goedecker, S.; Hutter, J. Relativistic separable dual-space Gaussian pseudopotentials from H to Rn. *Phys. Rev. B* **1998**, *58*, 3641.

https://doi.org/10.1021/acsomega.1c00869
ACS Omega 2021, 6, 12676−12683

(57) Martyna, G. J.; Tuckerman, M. E. A reciprocal space based method for treating long range interactions in *ab initio* and force-field-based calculations in clusters. *J. Chem. Phys.* **1999**, *110*, 2810−2821.
(58) Martyna, G. J.; Klein, M. L.; Tuckerman, M. E. Nosé-Hoover chains: The canonical ensemble via continuous dynamics. *J. Chem. Phys.* **1992**, *97*, 2635−2643.
(59) Laio, A.; Parrinello, M. Escaping free-energy minima. *Proc. Natl. Acad. Sci. U.S.A.* **2002**, *99*, 12562−12566.
(60) Iannuzzi, M.; Laio, A.; Parrinello, M. Efficient Exploration of Reactive Potential Energy Surfaces Using Car-Parrinello Molecular Dynamics. *Phys. Rev. Lett.* **2003**, *90*, No. 238302.
(61) Laio, A.; Gervasio, F. L. Metadynamics: a method to simulate rare events and reconstruct the free energy in biophysics, chemistry and material science. *Rep. Prog. Phys.* **2008**, *71*, No. 126601.
(62) Barducci, A.; Bonomi, M.; Parrinello, M. Metadynamics. *Wiley Interdiscip. Rev.: Comput. Mol. Sci.* **2011**, *1*, 826−843.
(63) Valsson, O.; Tiwary, P.; Parrinello, M. Enhancing Important Fluctuations: Rare Events and Metadynamics from a Conceptual Viewpoint. *Annu. Rev. Phys. Chem.* **2016**, *67*, 159−184.
(64) Ensing, B.; Laio, A.; Parrinello, M.; Klein, M. L. A Recipe for the Computation of the Free Energy Barrier and the Lowest Free Energy Path of Concerted Reactions. *J. Phys. Chem. B* **2005**, *109*, 6676−6687.
(65) Tripathi, R.; Glaves, R.; Marx, D. The GTPase hGBP1 converts GTP to GMP in two steps via proton shuttle mechanisms. *Chem. Sci.* **2017**, *8*, 371−380.
(66) Muñoz-Santiburcio, D.; Farnesi Camellone, M.; Marx, D. Solvation-Induced Changes in the Mechanism of Alcohol Oxidation at Gold/Titania Nanocatalysts in the Aqueous Phase versus Gas Phase. *Angew. Chem., Int. Ed.* **2018**, *57*, 3327−3331.
(67) Tripathi, R.; Noetzel, J.; Marx, D. Exposing catalytic versatility of GTPases: taking reaction detours in mutants of hGBP1 enzyme without additional energetic cost. *Phys. Chem. Chem. Phys.* **2019**, *21*, 859−867.
(68) Tripathi, R.; Forbert, H.; Marx, D. Settling the Long-Standing Debate on the Proton Storage Site of the Prototype Light-Driven Proton Pump Bacteriorhodopsin. *J. Phys. Chem. B* **2019**, *123*, 9598−9608.
(69) Barducci, A.; Bussi, G.; Parrinello, M. Well-Tempered Metadynamics: A Smoothly Converging and Tunable Free-Energy Method. *Phys. Rev. Lett.* **2008**, *100*, No. 020603.
(70) Torrie, G. M.; Valleau, J. P. Nonphysical sampling distributions in Monte Carlo free-energy estimation: Umbrella sampling. *J. Comput. Phys.* **1977**, *23*, 187−199.
(71) Sprik, M.; Ciccotti, G. Free energy from constrained molecular dynamics. *J. Chem. Phys.* **1998**, *109*, 7737−7744.

https://doi.org/10.1021/acsomega.1c00869
ACS Omega 2021, 6, 12676−12683